A Finite Element Analysis of Bearing Resistance of Timber Loaded through a Steel Plate

Awaludin, A.[1], Hirai, T.[2], Hayashikawa, T.[3], and Leijten, A.J.M.[4]

Abstract: Decrease projected length of bolts due to bending deformation in timber joints compresses the steel washers onto timber member and increases lateral resistance of the joints. As this lateral strength increase primarily depend on bearing characteristics of timber beneath the steel washers, a finite element analysis was performed to predict their bearing-embedment behavior. A 3-D finite element model consisting of 8-node solid and contact pair elements was developed using ANSYS assuming an anisotropic plasticity model for timber and an elastic-perfectly plastic model for the washers. Material constants for both steel washer and timber member were obtained from previous test data. The results of the analysis were in good agreement with the experimental load-embedment curves as well as the analytical curves obtained in a previous study based on a rigid-body-spring-model. The same approach was also used to evaluate the effective bearing length (under uniform compression) of a 50 mm depth timber block partially compressed.

Keywords: Bearing resistance, contact condition, effective bearing length, finite element model, partial compression.

Introduction

The mechanical behavior of bolted timber joints beyond the elastic limit is obviously affected by the development of axial forces in bolts as a result of bending deformation of the bolts. The axial force development has a positive effect on the (ultimate) lateral resistance, ductility and hysteretic response [1-3]. Some studies have considered this axial force in their numerical models [4-6]. Linear and non-linear spring elements were used in those numerical models and its behavior was determined based on the load-embedment curves of timber beneath steel washers or steel side plate. The embedment resistance of timber under steel washers should be considered in an appropriate design method of bolted timber joints with steel washers or side plates.

[1] Department of Civil and Environmental Engineering, Universitas Gadjah Mada, Jl. Grafika No. 2, UGM campus, Yogyakarta, 55281, INDONESIA.
E-mails: ali@tsipil.ugm.ac.id

[2] Research Faculty of Agriculture, Hokkaido University, Kita 9 Nishi 9, Kita-ku, Sapporo 060-8589, JAPAN.

[3] Research Faculty of Engineering, Hokkaido University, Kita 13 Nishi 8, Kita-ku, Sapporo 060-8628, JAPAN.

[4] Department of Architecture, Building and Planning, Eindhoven University of Technology, Den Dolech 2, P.O. Box 513, VRT 9.23, 5600 MB Eindhoven, THE NETHERLANDS.

An attempt to analyze numerically the bearing resistance of steel washers on timber members using rigid-body-spring-model (RBSM) was previously presented by Hirai et al [7]. In their analysis a steel washer was assumed to consist of discrete rigid plate elements connected to adjacent elements with springs and supported on foundation springs at their centers of gravity. The foundation springs were determined by considering an effective foundation area for partial bearing under rigid bodies [7], which varied upon loading configuration [8-10]. They ignored shear contribution of deformed timber fibers as Winkler-type foundation springs were used in their numerical model. In this study the load-embedment curve of the steel washer on timber was simulated using the ANSYS v.10 [11] based on a 3-D finite element model consisting of 8-node solid and contact pair elements. The same technique was used to study the effective bearing length of timber member under partial bearing just like contact joints between columns and sills.

Finite Element Modeling

The experimental model shown in Fig. 1, which was adopted from the work of Hirai et al [7], was used in this finite element analysis. The timber species used in the above work was *Picea jezoensis*. The specimens had an average moisture content of 13.1% and air-dry specific gravity of 0.41. Both steel washer and timber member had a pre-drilled hole of 13 mm diameter and were discretized using 8-node solid elements as shown in Fig. 2.
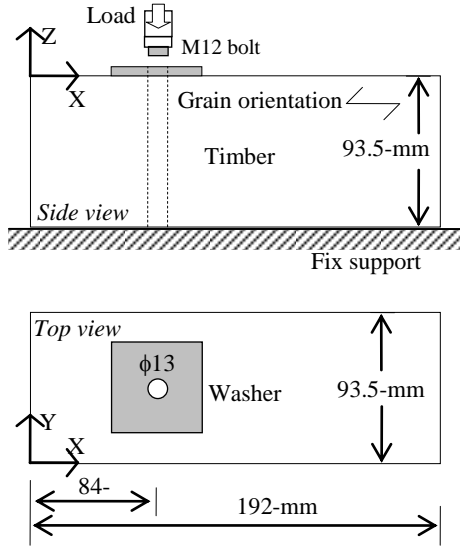
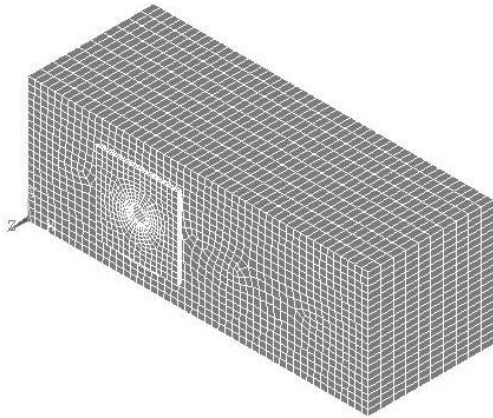**Figure 1.** Bearing Test Model of Timber Member Under Steel Washer [7]

Figure 2. A 3-D Finite Element Model for Timber Bearing Under Steel Washer in ref. 7

The axial force perpendicular to the timber grain was facilitated by applying uniform nodal force to nodes at the presence of M12 bolt head around the bolt-hole of the washer. A flexible surface-to-surface contact model was implemented via contact pair of CONTA174 and TARGE170 elements provided by the finite element codes ANSYS v.10 [11]. The normal and sliding contact stiffness was automatically calculated based on the material properties of the underlying elements and was updated on each step of the computation. In this analysis, the static frictional coefficient between the steel washer and the timber member was roughly assumed as 0.3 [6].

A bilinear stress-strain relationship was assumed for each anisotropic axis of timber. An apparent yield stress and tangent modulus are required for each stress-strain relationship. Therefore, 18 additional constants are needed in addition to the 9 normally required for orthotropic elastic material. These

constants are summarized in Table 1 [12]. E_x, E_y, E_z are moduli of elasticity in three material axes; G_{xy}, G_{yz}, G_{xz} are shear moduli; E_t is tangent modulus; G_t is tangent shear modulus; $\sigma_\pm$ is yield stress in tension or compression; τ is shear stress and ν is Poisson's ratio. It was further assumed that the maximum stress criterion was used so that at each load increment the three normal stresses and shear stresses are independently compared against critical values; little or no interaction between these stresses exists [13].

Table 1. Material Constants for Timber used in the Finite Element Model [12]

E_x	4,720 MPa	G_{txz}	9.5 MPa
E_y	378 MPa	$\sigma_{\pm x}$	18 MPa
E_z	236 MPa	$\sigma_{\pm y}$	3.72 MPa
G_{xy}	337 MPa	$\sigma_{\pm z}$	3.72 MPa
G_{yz}	33.7 MPa	τ_{xy}	4.08 MPa
G_{xz}	317 MPa	τ_{yz}	0.93 MPa
$E_{t\pm x}$	140 MPa	τ_{xz}	3.09 MPa
$E_{t\pm y}$	11 MPa	ν_{xy}	0.37
$E_{t\pm z}$	7 MPa	ν_{yz}	0.47
G_{txy}	10 MPa	$\nu_{\xi\zeta}$	0.42
G_{tyz}	1 MPa		

The yield stresses in three material axes are not independent to each others, but they must satisfy the consistency equation described as

$$\frac{\sigma_{tx} - \sigma_{cx}}{\sigma_{tx}\sigma_{cx}} + \frac{\sigma_{ty} - \sigma_{cy}}{\sigma_{ty}\sigma_{cy}} + \frac{\sigma_{tz} - \sigma_{cz}}{\sigma_{tz}\sigma_{cz}} = 0 \qquad (1)$$

where σ_{tx} and σ_{cx} refer to x-direction yield stress in tension and compression, respectively.

The washer was modeled as elastic-perfectly plastic and its material properties obtained from direct tests [7] were: E = 195 GPa; σ_{yield} = 308.7 MPa; ν = 0.3.

Results and Discussions

Figure 3 shows the load-embedment curves up to 5 mm embedment of the FEM analysis for three square steel washers of 40x40 mm (sw-40), 60x60 mm (sw-60) and 80x80 mm (sw-80) and a circular washer of 25 mm diameter (cw-25). All washers have thickness equals to 4.3 mm. The FEM curves clearly indicate that bearing load increases with washer dimension and the circular washer cw-25, which has the smallest surface (contact) area among the four kinds of considered washers, yields the lowest bearing load at a same embedment.

Figure 4, 5 and 6 show the load-embedment curves of the FEM analysis as well as the curves from the experiments and those given by Hirai et al [7] (marked as RBSM) for the steel washers sw-40, sw-60 and sw-80. Some test data at early stage of

loading was removed from the experimental curves as they generally produce initial slip with no bearing load. As a result, comparison between experimental and predicted load-embedment curves at initial loading becomes more convenience. The predicted curves given by FEM and RBSM analyses are in good agreement with experimental data especially with steel washer sw-60 and sw-80. FEM curve differed from the RBSM curve only for the steel washer sw-40 (see Fig. 4), where a notable variation was also observed among the load-embedment curves of the experimental results. Further investigation is required for specimens with steel washer sw-40 including more experimental data as to clarify this discrepancy.
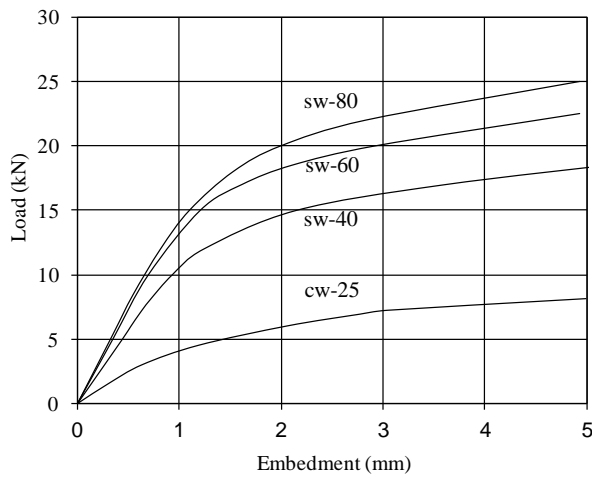

Figure 5. Experimental and Predicted Load-Embedment Curves, Washer sw-60

Figure 3. FEM Predicted Load-Embedment Curves for four Kinds of Steel Washer (sw-40, square washer 40x40 mm; sw-60x60, square washer 60x60 mm; sw-80, square washer 80x80 mm; and cw-25, circular washer 25 mm diameter)
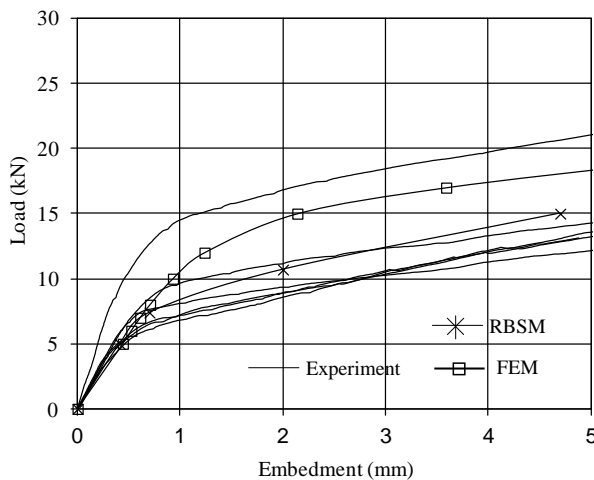

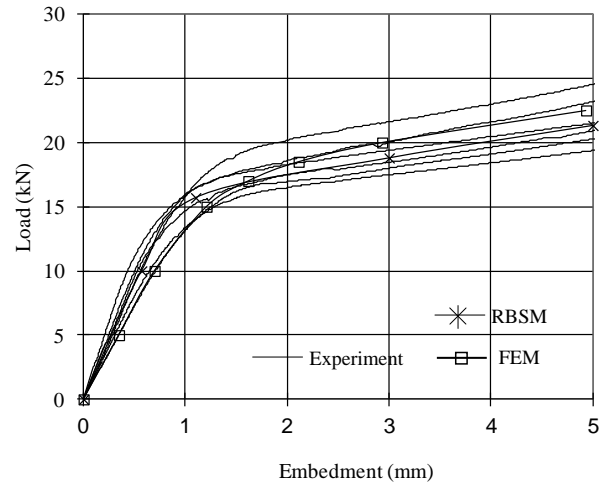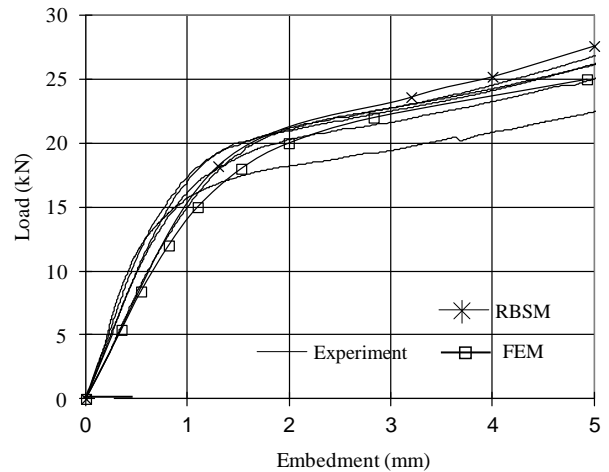**Figure 6.** Experimental and Predicted Load-Embedment Curves, Washer sw-80

Numerical Simulation

Some numerical simulations were conducted using the FEM model developed above.

Rigid Body Assumption

If steel plates have enough thickness, they can practically be regarded as rigid bodies that introduce uniform embedment on timber members. Precise information about dimensional proportions of the plates that ensure the quasi-rigid behavior, however, has not been available. In this study, therefore, the effect of width/thickness ratio was simulated first. Figure 7 shows a 50 mm depth timber block under two different loading conditions, partial and uniform compression.
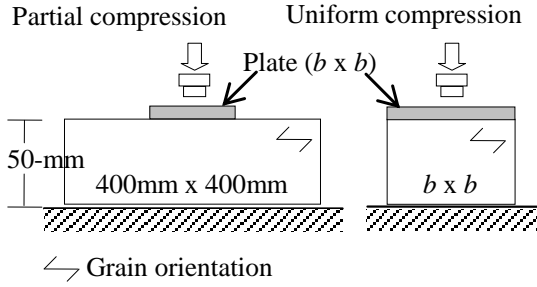

Figure 4. Experimental and Predicted Load-Embedment Curves, Washer sw-40

Partial compression　**Uniform compression**

Plate (*b* x *b*)

50-mm

400mm x 400mm　　*b* x *b*

Grain orientation

Figure 7. Timber Block Model for the Evaluation of Rigid Body Assumption (*b*: plate width)

In the block with a partial compression, the block dimension in grain direction or perpendicular is 400 mm, while in the block with a uniform compression the block dimension is exactly the same as the dimension of the steel plate. In both loading conditions, the steel plate thickness is made constant, 10 mm, while the plate width (*b*) is defined according to the selected width-over-thickness ratio. And the load is assumed as uniform nodal forces within an area of M12 bolt head (15 mm by 15 mm) at the center of the plate.

An ideal rigid plate has a uniform embedment, which means the plate rigidity ratio, *r*, expressed by Eq. (2) equals to zero.

$$r = \frac{(\delta_{max} - \delta_{min})}{\delta_c} \times 100\% \qquad (2)$$

In Eq. (2), δ_{max} and δ_{min} is, respectively, maximum and minimum embedment of the plate and δ_c is embedment of the center of the plate. Our finite element analysis results indicate that *r* is less than 5% when plate width-over-thickness ratio is not higher than 6 under partial compression or 9 under uniform compression, respectively. Blocks under partial compression introduce bending by lateral forces distributed along the block edges. Therefore, thicker plates are required to attain the same level of *r* which is calculated for the case of the uniform compression.

Effective Length under Partial Bearing

Under partial bearing the effective bearing length, which corresponded to the bearing length with uniform compression, was simulated assuming the load transmission through a rigid body. The effective bearing length has been proposed in many previous studies [7, 14] to evaluate the ultimate effective (equivalent) partial compressive strength. The effective bearing length was simulated using the same technique. In this study, a block loaded as shown in Fig. 8 was considered. The block dimension and loading arrangement is adhered to ASTM D143 [15]

and the plate can be assumed as rigid body (width-over-thickness ratio equals to 4.2).

Figure 9(a) shows the analytical bearing stress-strain curves for various margins, while Fig. 9(b) shows the analytical curves obtained from six different depths of the block (*d*, 50 mm; 75 mm; 100 mm; 125 mm; 150 mm and 200 mm) under two kinds of loading condition. Here bearing stress is force perpendicular to the timber grain divided by the plate (contact) area, and strain is defined as plate embedment divided by block depth.
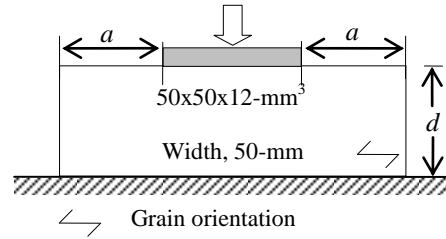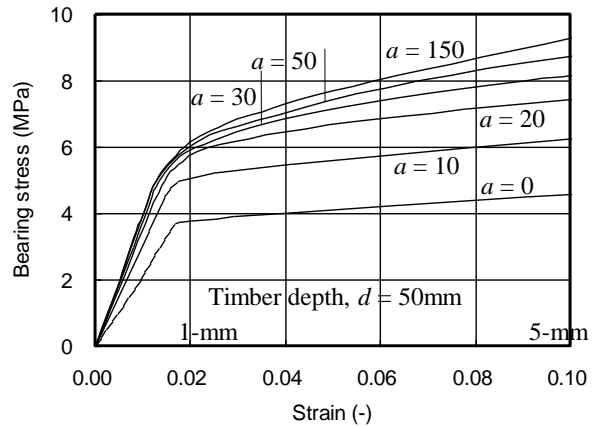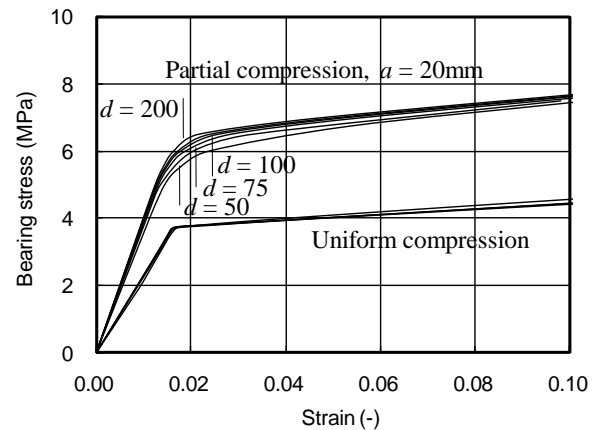
a　　　　*a*

50x50x12-mm³

d

Width, 50-mm

Grain orientation

Figure 8. Model of Block Under Partial Bearing (*d*: timber depth; *a*: margin)

(a) Various margin

(b) Various depth

Figure 9. Analyzed Bearing Stress-Strain Curves (*d*: timber depth; *a*: margin)

For a compressive strain equals to 2% known as serviceability limit [14] a significant increase of bearing load for 10 mm or 20 mm margin is well observed in Fig. 9(a). But for margin more than 20 mm, the increase comes down. For a very large margin (a equals to 150 mm), the bearing stress corresponding to 2% of strain is about 1.6 times the bearing stress under uniform compression (a equals to zero). This suggests that the bearing load can be attained by assuming effective bearing length (under uniform compression) of 80 mm, which is 1.6 times the actual width of the plate (50 mm). This increase of effective bearing length from 50 mm to 80 mm can also be achieved by assuming 1:3 stress dispersion as proposed by a previous study [16]. This stress dispersion means that for a timber depth equals to d, the effective bearing length can be extended by one third of d to the left and right sides. However, if the 5 mm embedment is adopted as the limit for thin timber members [17] the slope of stress dispersion changes into 1:2.

From stress-strain curves shown in Fig. 9(b), the influence of timber depth is noticed in the block with partial compression but it is less obvious for the blocks with uniform compression. No influence of timber depth on bearing stress-strain curve of the blocks under uniform compression is confirmed by the experiment of a previous study [14]. In partially compressed blocks, increasing the depth from 50 mm to 125 mm yields a proportional increase at 2% strain. However, increasing the block depth over 125-mm-depth yields a very small increase of the load at a same strain. This increase is about 7% and 10.5%, for depth changing from 50 mm to 125 mm and from 50 mm to 200 mm, respectively. However, for a strain equals to 10%, increasing the depth of the block from 50 mm to 125 mm has no effect as shown in Fig. 9(b).

Conclusions

In this study a 3-D finite element model was developed using ANSYS to predict the bearing load-embedment curve of a steel washer on a timber member which is necessary to incorporate the development of axial forces into an appropriate design model of laterally loaded bolted joints. A flexible surface-to-surface contact model having static frictional coefficient of 0.3 was included into the FEM to consider the contact condition between the washer and timber. The numerical results showed that the bearing load increases with washer dimension and the predicted load-embedment curves are in good agreement with experimental data. In addition, this study confirms the results of previous studies that a slope of stress dispersion of 1:3 and 1:2 can be practically assumed to evaluate the effective

bearing length of timber under partial compression at 2% and 10% strain, respectively.

Acknowledgement

References

1. Awaludin, A., Hirai, T., Hayashikawa, T., Sasaki, Y. and Oikawa, A., Effects of Pretension in Bolts on Hysteretic Response of Moment-carrying Timber Joints, *Journal of Wood Science*, 54, 2008, pp. 114-120.

2. Awaludin, A., Hayashikawa, T., Oikawa, A., Hirai, T., Sasaki, Y., and Leijten, A.J.M, Seismic Properties of Moment-resisting Timber Joints with a Combination of Bolts and Nails, *Civil Engineering Dimension*, 13(1), 2011, pp. 1-5.

3. Awaludin, A., Hirai, T., Sasaki, Y., Hayashikawa, T., Oikawa, A., Beam-to-column Timber Joints with Pretensioned Bolts, *Civil Engineering Dimension*, 13(2), 2011, pp. 59-64.

4. Hirai, T., Nonlinear Load-slip Relationship of Bolted Wood-Joints with Steel Side-Member II: Application of the Generalized Theory of a Beam on an Elastic Foundation, *Mokuzai Gakaishi*, 29, 1983, pp. 839-844.

5. Schreyer, A.C., *Monotonic and Cyclic Behavior of Slender Dowel-type Fasteners in Wood-steel-wood Connections*. M.A.Sc. Thesis, Department of Wood Science, The University of British Columbia, 2002.

6. Awaludin, A., Hirai, T., Hayashikawa, T., Sasaki, Y., Load-carrying Capacity of Steel-to-timber Joints with a Pretensioned Bolt, *Journal of Wood Science*, 54, 2008, pp. 362-368.

7. Hirai, T., Tsujino, T., Sasaki, Y., Steel Washer on Timber, *Proceedings of World Conference on Timber Engineering*, August 6-10, Portland, 2006. (CD-ROM)

8. Inayama, M., *Theory of Embedment of Timber and its Application*, Ph.D. Thesis, The University of Tokyo, 1991.

9. Kawamoto, N. and Kanaya, N., Elastic Deformation of Wood Subjected to Compression Perpendicular-to-the-grain. Effects of Length and Depth of Specimen, and Effect of Contact Length of Bearing Plate on an Elastic Foundation, *Mokuzai Gakaishi*, 37, 1991, pp. 16-23.

10. Leijten, A. J. M., Larsen, H. J., Van der Put T. A. C. M., Structural Design for Compression Strength Perpendicular to the Grain of Timber

Blocks, *Journal of Construction and Building Materials*, 24, 2010, pp. 252-257.

11. Swanson Analysis System Inc., *ANSYS v.10.*, Swanson Analysis System Inc., Houston, Pa, 1996.

12. Awaludin, A., Toshiro Hayashikawa, T., Hirai, T., Sasaki, Y., Loading Resistance of Bolted Timber Joints beyond their Yield-loads, *Proceedings of the 2nd ASEAN Civil Engineering Conference*, March 11-12, Vientiane, 2010, pp. 148-158.

13. Moses, D. M., Prion, H. G L., A Three-dimensional Model for Bolted Connection in Wood, *Canadian Journal of Civil Engineering*, 30, 2003, pp. 555-567.

14. Blass, H. J., and Gorlacher, R., Compression Perpendicular to the Grain, *Proceedings of World Conference on Timber Engineering*, June 14-17, Finland, 2004. (CD-ROM)

15. *American Society for Testing and Materials: Standard test methods for small clear specimens of timber, ASTM D143*, American Society of Testing and Materials, Philadelphia, 1994.

16. Madsen, B., Proposal for Including an Updated Design Method for Bearing Stresses in CIB-W18 Structural Design Code, *Proceedings of the 22nd CIB-W18*, Berlin, 1989.

17. Riberholt, H., *Compression Perpendicular to the Grain of Wood*, COWI-report P-42239-1, 2000.